Synthesis, differential thermal analysis, and crystal structure of the quaternary chalcogenide compound $Cu_2FeGeTe_4$

G. E. Delgado[a,*], E. Quintero[b], P. Delgado-Niño[c], R. Guillén-Guillén[d], and G. Márquez[e]

[a]*Laboratorio de Cristalografía, Departamento de Química, Facultad de Ciencias, Universidad de Los Andes, Mérida, 5101, Venezuela,*
[*]*e-mail: gerzon@ula.ve*
[b]*Centro de Estudios de Semiconductores, Departamento de Física, Facultad de Ciencias, Universidad de Los Andes, Mérida 5101, Venezuela.*
[c]*Facultad de Ingeniería Industrial, Universidad Distrital Francisco José de Caldas, Bogotá 111071, Colombia.*
[d]*Departamento General de Ciencias, Universidad Continental, Arequipa 04002, Perú.*
[e]*Instituto de Energías Renovables, Universidad Tecnológica del Perú, Arequipa 04001, Perú.*

Received 23 March 2025; accepted 11 July 2025

This study reports on the quaternary diamond-like semiconductor copper iron germanium tellurium, $Cu_2FeGeTe_4$. The material was synthesized using the melt and annealing technique by directly reacting the elements. The thermal behavior of the $Cu_2FeGeTe_4$ compound was investigated using thermogravimetric analysis. The Rietveld refinement method characterized the crystal structure through X-ray powder diffraction. The powder diffraction pattern revealed that the principal phase, $Cu_2FeGeTe_4$, constituted 85.4%, while the secondary phase, $FeTe_2$, accounted for 14.6%. The quaternary chalcogenide compound $Cu_2FeGeTe_4$ belongs to the I_2-II-IV-VI_4 system and crystallizes in the stannite structure within the non-centrosymmetric tetragonal space group $I\text{-}42m$ (N° 121), Z = 2, with unit cell parameters $a = 5.9293(8)$ Å, $c = 11.9239(8)$ Å, $V = 419.20(2)$ Å^3. Its structure consists of a three-dimensional close-packed arrangement of slightly distorted $CuTe_4$, $FeTe_4$, and $GeTe_4$ tetrahedra, interconnected through shared faces and corners. The chemical structure was verified through Bond Valence Sum (BVS) calculations.

Keywords: Chalcogenide; chemical Synthesis; thermal analysis; powder X-ray diffraction; crystal structure; Rietveld method; bond valence sum.

DOI: https://doi.org/10.31349/RevMexFis.72.010503

1. Introduction

Diamond-like semiconductors can be formed by cross substitution in the cationic sublattice starting from the basic structures of diamond. Most semiconductor compounds crystallize in tetrahedral structures, characterized by tetrahedral bonds. These bonds require an average of four valence electrons per atom, and the total valence electrons per anion must total eight [1]. Additionally, these compounds must adhere to Pauling's second rule, which states that the charge of the anion must be compensated by its nearest neighboring cations [2].

Quaternary diamond-like compounds with formula I_2-II-IV-VI_4 satisfy the rules of adamantane compound formation. Due to their wide variety of possible compositions (I= Cu, Ag, II= Zn, Cd, Mn, Fe, IV= Si, Ge, Sn, VI= S, Se, Te), these materials have significant potential applications in fields such as solar cell semiconductors [3], photovoltaics [4], spintronics [5], non-linear optics [6], and thermoelectrics [7].

Two primary structural types have been reported for this quaternary family of compounds; sphalerite derivative structures and wurtzite derivative structures. The sphalerite derivatives possess tetragonal symmetry; with structures such as Cu_2FeSnS_4-type (stannite, space group $I\text{-}42m$), or Cu_2ZnSnS_4-type (kesterite, space group $I\text{-}4$) [8]. In contrast, the würtzite derivatives exhibit either orthorhombic symmetry, as in Cu_2CdGeS_4-type (würtzite-stannite, space group $Pmn2_1$) [9] or monoclinic symmetry, as in Na_2ZnSiO_4-type (würtzite-kesterite, space group Pc) [10]. More recently, the diamond-like compound Ag_2CdGeS_4 has been shown to crystallize in the orthorhombic space group $Pna2_1$ [11], representing a new polymorph compared to the previously reported structure in the $Pmn2_1$ space group [9–12]. These crystallographic variations arise from differences in cation distribution within the tetrahedral sites.

Among this family of compounds, the p-type semiconductor $Cu_2FeGeTe_4$ is particularly interesting. Its preparation and magnetic properties were previously reported [13, 14]. The general composition diagram for the Cu-Fe-Ge-Te system is shown in Fig. 1, where the compound $Cu_2FeGeTe_4$ corresponds to Cu (I)= 0.25, Fe (II)= Ge (IV)= 0.125, and Te (VI)= 0.5.

This material exhibits ferromagnetic properties with a Néel temperature of T_N = 160.1 K [13]. However, its crystal structure has not been fully established. Earlier studies using photographic Güinier data suggested an orthorhombic cell with parameters a= 7.656 Å, b= 6.567 Å, and c= 6.506 Å, though no structural details were provided [14]. To further investigate the crystalline structures of diamond-like compounds [15–20], this study reports the synthesis, thermal

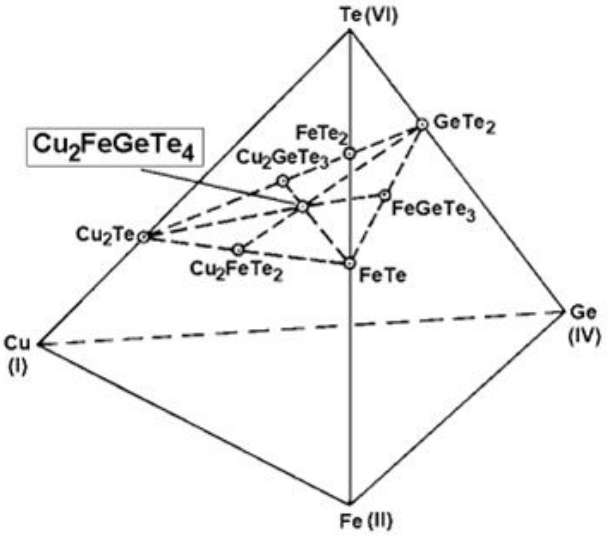

FIGURE 1. Compositional representation of the Cu-Fe-Ge-Te quaternary solid solution system.

analysis, and crystal structure using the Rietveld method from powder X-ray diffraction data of the chalcogenide compound $Cu_2FeGeTe_4$.

2. Experimental

2.1. Synthesis

The quaternary compound was synthesized using the melt and annealing technique. High-purity starting materials (Cu, Fe, Ge, and Te; 99.99 wt%) were mixed in stoichiometric ratios and sealed in an evacuated quartz tube ($\sim 10^{-4}$ Torr). Specifically, were mixed 142.35 mg of Cu (2.24 mmol), 107.23 mg of Fe (1.92 mmol), 81.35 mg of Ge (1.12 mmol), and 775.41 mg of Te (6.08 mmol) until completing almost 1 gram of mixture (1106.34 mg). The inner walls of the quartz tube were subjected to pyrolysis to prevent reactions between the starting materials and the quartz. The fusion process was conducted in a furnace, gradually heated to 1150°C at 20°C/h. The ampoule was mechanically shaken during heating to ensure complete mixing of the elements. The maximum temperature (1150°C) was maintained for 48 hours with continuous shaking. Afterward, the shaking system was turned off, and the temperature was gradually reduced to 20°C/h until reaching 500°C. The ampoule was held at this temperature for 30 days before cooling to room temperature at 10°C/h. The sample was examined under the microscope, revealing that the ingot was homogeneous throughout.

2.2. Chemical analysis

The sample's stoichiometric composition was analyzed using a Hitachi S2500 scanning electron microscope (SEM) equipped with a Kedex energy-dispersive X-ray (EDX) accessory. Three distinct regions of the ingot were checked, and the error margin in the standardless analysis was approximately 5%.

2.3. Differential thermal analysis

The thermal properties of the title compound were obtained in the temperature range between 20 and 1000°C using a Perkin-Elmer DTA-7 device with gold as reference material. The charge of the powdered alloy was approximately 100 mg weight. The sample underwent both heating and cooling runs. The average rate of these runs was approximately 10°C/min. The error in determining these temperatures is about ± 10°C.

2.4. Powder X-ray diffraction

A small portion of the ingot was ground using an agate mortar and pestle to prepare a fine powder for X-ray diffraction analysis. The powder was mounted on a flat zero-background holder coated with a thin layer of petroleum jelly. Data were collected at 293(1) K using a Siemens D5005 diffractometer (CuKα_1 radiation: λ = 1.54059 Å; 40 kV, 30 mA) with a Ge<111> primary monochromator. A fixed aperture and divergence slit (1 mm), a 1 mm monochromator slit, and a 0.1 mm detector slit were used. The sample was scanned from 10° to 100° 2θ, with a step size of 0.02° and a counting time of 20 s per step. Quartz was employed as an external standard to determine the 2θ-zero correction. WinPlotr software [21] was used to establish peak positions and intensities.

3. Results and discussion

Figure 2 presents the thermogram of the title compound. In the temperature range from room temperature to 755 K, the sample remains in the solid phase, consisting of the low-temperature modification of $Cu_2FeGeTe_4$ and a secondary phase, $FeTe_2$, as confirmed by powder X-ray diffraction anal-

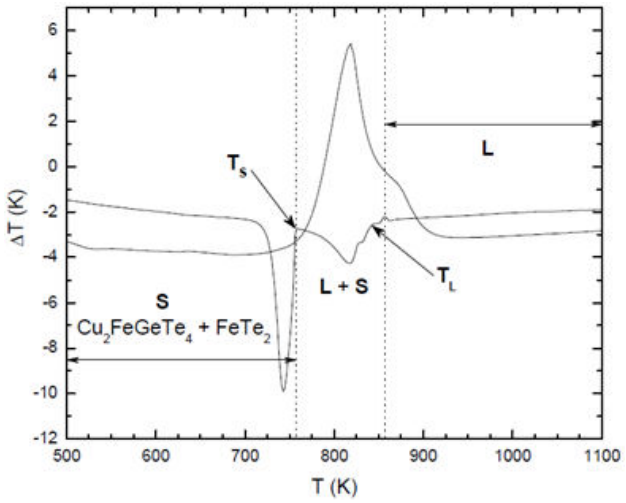

FIGURE 2. DTA thermogram for $Cu_2FeGeTe_4$.

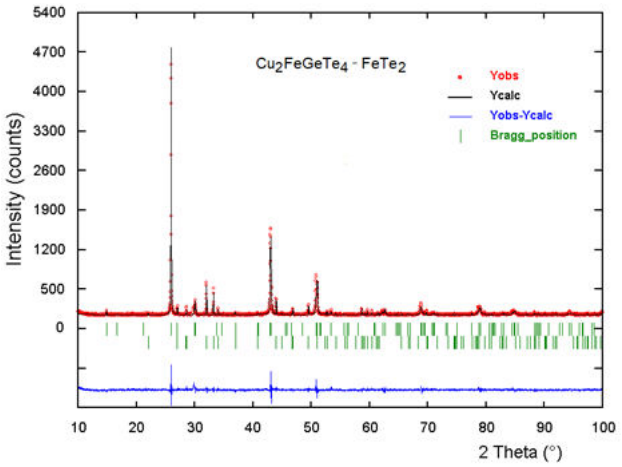

FIGURE 3. Rietveld refinement final plot of $Cu_2FeGeTe_4$. The lower trace shows the difference between the observed and calculated patterns. Vertical bars indicate the Bragg reflections.

ysis. Between 755 K and 850 K, a two-phase region (liquid + solid, L + S) is proposed. The solid (S) phase likely comprises binary $FeTe_2$ along with a probable high-temperature modification of $Cu_2FeGeTe_4$. The transition to liquid phase (L) occurs at approximately 850 K. Due to irregularities observed in the thermogram, the liquidus temperature (TL) is estimated at 840 ± 10 K, while the solidus temperature (TS) is approximately 760 ± 10 K. These findings contribute to understanding the phase stability and melting behavior of $Cu_2FeGeTe_4$, which is relevant for its potential applications in thermoelectric and electronic materials.

Figure 3 presents the X-ray powder diffractogram of the $Cu_2FeGeTe_4$ compound. An automatic search in the PDF-ICDD database, set 1-73 [22], using the software provided with the diffractometer, revealed that the powder pattern contained small amounts of the binary $FeTe_2$ (PDF No. 14-419). The Bragg positions of the diffraction lines corresponding to this compound are also marked in Fig. 3. The first 20 peak positions of the main phase ($Cu_2FeGeTe_4$) were indexed using the Dicvol04 program [23], which provided a unique solution in a tetragonal unit cell. In addition, a systematic absences study ($hkl : h + k + l = 2n$) confirmed an I-type cell.

The complete powder diffraction dataset for Cu_2FeGeT_4 was analyzed using the NBS*AIDS program [24], yielding the following results: unit cell parameters $a = 5.925(1)$ Å,

TABLE I. X-ray powder diffraction data for $Cu_2FeGeTe_4$.

$2\theta_{obs}$ (°)	d_{obs} (Å)	$(I/I_0)_{obs}$	h	k	l	$2\theta_{cal}$ (°)	d_{cal} (Å)	$\Delta 2\theta$ (°)
15.997	5.5358	1.3	0	0	2	16.022	5.5273	0.025
17.739	4.9959	2.6	1	0	1	17.741	4.9954	0.002
27.679	3.2203	100.0	1	1	2	27.691	3.2189	0.012
31.918	2.8016	2.6	2	0	0	31.938	2.7998	0.020
45.804	1.9794	20.7	2	2	0	45.794	1.9798	-0.010
46.121	1.9665	35.1	2	0	4	46.113	1.9669	-0.008
54.356	1.6864	15.6	3	1	2	54.359	1.6863	0.003
54.917	1.6705	11.5	1	1	6	54.920	1.6705	0.003
57.215	1.6088	2.5	2	2	4	57.190	1.6094	-0.025
66.776	1.3998	4.4	4	0	0	66.767	1.3999	-0.009
67.764	1.3817	4.0	0	0	8	67.759	1.3818	-0.005
73.762	1.2835	4.7	3	3	2	73.744	1.2838	-0.018
74.224	1.2766	7.2	3	1	6	74.220	1.2767	-0.004
84.967	1.1405	7.1	4	2	4	84.968	1.1405	0.001
85.626	1.1334	5.2	2	2	8	85.656	1.1331	0.030
91.290	1.0773	1.7	5	1	2	91.308	1.0771	0.018
91.762	1.0730	1.7	3	3	6	91.766	1.0730	0.004
92.681	1.0647	1.3	1	1	10	92.681	1.0647	0.000
102.198	0.9898	1.1	4	4	0	102.185	0.9899	-0.013
103.142	0.9833	1.5	4	0	8	103.122	0.9834	-0.020
109.003	0.9462	1.3	5	3	2	109.002	0.9462	-0.001
110.470	0.9377	1.3	3	1	10	110.459	0.9377	-0.011
120.903	0.8855	1.3	6	2	0	120.919	0.8854	0.016
123.344	0.8751	1.3	2	0	12	123.349	0.8751	0.005

TABLE II. Rietveld refinement results for $Cu_2FeGeTe_4$ and $FeTe_2$.

Chemical formula	$Cu_2FeGeTe_4$	$FeTe_2$
Formula weight (g/mol)	765.95	183.45
a (Å)	5.9293(2)	3.821(3)
c (Å)	11.9239(4)	6.275(3)
V (Å^3)	419.20(2)	91.6(1)
$\eta = c/2a$	1.00	-
System	tetragonal	tetragonal
Space group	$I\bar{4}2m$ (N°121)	$P4/nmm$ (N°129)
Z	2	2
D_{calc} (g/cm^3)	6.07	6.65
Weight fraction (%)	85.4	14.6
	R_{exp} (%) = 6.9	R_p (%) = 7.0
	R_{wp} (%) = 8.6	S = 1.2

$c = 11.93(1)$ Å, and figures of merit M_{20} = 52.5 [25] and $F_{20} = 22.1$ (0.0111, 98) [26]. The X-ray powder diffraction data for $Cu_2FeGeTe_4$ are summarized in Table I, which includes the observed and calculated 2θ values, d-spacings, and relative intensities of the reflections.

Based on the sample composition, unit cell parameters, and body-centered cell, a revision of the diffraction lines of the main phase confirms that this material shares the same structure as the stannite-type compound, which crystallizes in the tetragonal space group I-$42m$ (No. 121) [8]. This structure type can serve as a reference model to refine the structure under investigation.

The Rietveld refinement [27] was performed using the FullProf program [28]. The atomic coordinates of the original stannite structure Cu_2FeSnS_4 [8] were used as the starting model for the quaternary $Cu_2FeGeTe_4$, with unit cell parameters obtained from the NBS*AIDS refinement. The atomic positions of the $FeTe_2$ binary [29] were incorporated as a secondary phase in the refinement. The angular dependence of the full width at half maximum (FWHM) was modeled using Caglioti's formula [30]. Peak shapes were described using the parameterized Thompson-Cox-Hastings pseudo-Voigt profile function [31]. Background variation was accounted for using a six-coefficient polynomial, while the thermal motion of the atoms was modeled with a single overall isotropic temperature factor.

Table II summarizes the Rietveld refinement results for $Cu_2FeGeTe_4$ and the secondary phase $FeTe_2$. The refinement parameters are defined as follows:

$$R_{\text{exp}} = 100\left[(N-P+C)/\sum w(y_{\text{obs}}{}^2)\right]^{1/2},$$

where $(N-P+C)$ is the number of degrees of freedom.

$$R_{\text{wp}} = 100\left[\sum w|y_{\text{obs}} - y_{\text{calc}}|^2/\sum w|y_{\text{obs}}|^2\right]^{1/2},$$

$$R_p = 100\sum |y_{\text{obs}} - y_{\text{calc}}|/\sum |y_{\text{obs}}|,$$

$$S = R_{\text{wp}}/R_{\text{exp}}.$$

Figure 3 shows the observed, calculated, and difference profiles for the final cycle of the Rietveld refinement. Table III shows the atomic coordinates, thermal displacement factors, bond distances, and angles for $Cu_2FeGeTe_4$. The unit cell diagram for this quaternary compound is shown in Fig. 4.

The semi-quantitative analysis from the Rietveld refinement [32] indicates that the sample consists of 85.4% $Cu_2FeGeTe_4$ and 14.6% $FeTe_2$. To compare the chemical analysis results with the Rietveld results, atomic percentages were calculated from the above values giving the following results: Cu (21.54%), Fe (15.35%), Ge (10.80%), and Te (52.31%). These results are close to those of the average atomic percentages obtained with EDX: Cu (21.5%), Fe (14.9%), Ge (10.6%), and Te (53.0%).

The Bond Valence Sum (BVS) theory is a simple yet powerful empirical method used to estimate the oxidation state (valence) of an atom in a crystal structure based on the lengths of its bonds [33]. The BVS values, for $Cu_2FeGeTe_4$, were calculated using the Brown-Altermatt empirical expression: V_{ij} = exp[($R_o - d_{ij}$)/B, where V_{ij} is the sum of all bonds between atom i and neighboring atoms j, R_o are the

TABLE III. Unit cell parameters, atomic coordinates, site occupancy factor, isotropic temperature factors, and selected geometric parameters (Å, °) for $Cu_2FeGeTe_4$.

Atom	Ox.	BVS	Wyck.	x	y	z	SOF	B (Å^2)
Cu	+1	1.35	4d	0	1/2	1/4	1	0.7(3)
Fe	+2	2.40	2a	0	0	0	1	1.1(1)
Ge	+4	3.68	2b	0	0	1/2	1	2.1(1)
Te	-2	2.37	8i	0.2539(9)	0.2539(9)	0.1259(9)	1	0.9(2)

Cu - Te	2.566(8)		Fe - Te	2.605(8)		Ge - Te^{i}	2.552(8)	
Te - Cu - Te^{ii}	109.6(2)	x4	Te - Fe - Te^{iv}	109.4(2)	x4	Te^{i} - Ge - Te^{iv}	107.9(2)	x4
Te - Cu - Te^{iii}	109.4(2)	x2	Te - Fe - Te^{v}	109.6(2)	x2	Te^{iv} - Ge - Te^{vi}	110.3(2)	x2

Symmetry codes: (^{i}) -0.5+x, -0.5+y, 0.5+z; (^{ii}) -y, x, -z; (^{iii}) -x, -y, z; (^{iv}) -0.5+y, 0.5-x, 0.5-z; (^{v}) -x, 1-y, z; (^{vi}) 0.5-y, -0.5+x, 0.5-z.
Bond valence sum (BVS): $V_{ij} = \sum_j \exp[(R_o - R_{ij})/b]$, r_o(Cu-Te)= 2.27 Å, r_o(Fe-Te)= 2.53 Å, r_o(Ge-Te)= 2.56 Å.

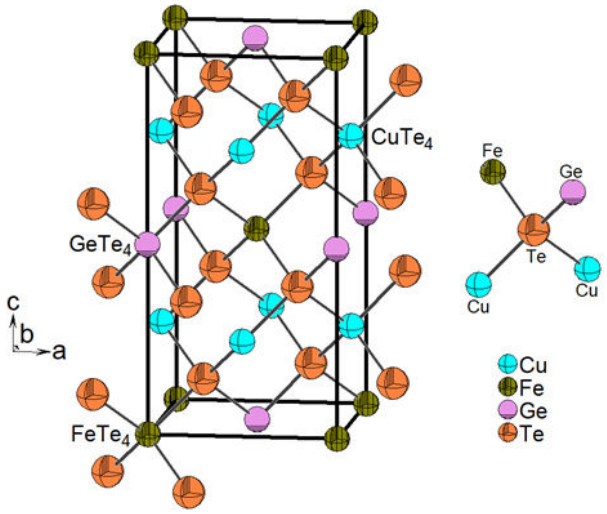

FIGURE 4. Unit cell diagram of $Cu_2FeGeTe_4$ showing the tetrahedra surrounding the cations (Cu, Fe, Ge) and anions (Te).

values for the reference distances, d_{ij} is the interatomic distance and B is universal constant (0.37 Å) [34]. The calculated oxidation states are consistent with the expected formal oxidation states, Cu^{+}, Fe^{2+}, Ge^{4+}, and Te^{2-}, as detailed in Table III. A deviation of ± 0.4 valence units from the expected oxidation state is typically considered acceptable [35].

The chalcogenide quaternary compound $Cu_2FeGeTe_4$ has a normal adamantane structure. It can be defined as a derivative of the sphalerite structure with a cubic closest-packed array of tellurium anions with Cu, Fe, and Ge occupying tetrahedral holes [1]. Figure 4 shows the unit cell diagram for this compound, where each cation is coordinated by four anions (Te) and each anion is coordinated by four cations (two Cu, one Fe, and one Ge) located at the corners of slightly distorted tetrahedrons. In $Cu_2FeGeTe_4$ all tellurium anions follow Pauling's second rule [2]. Its structure consists of a three-dimensional close-packed arrangement of lightly distorted $CuTe_4$, $FeTe_4$, and $GeTe_4$ tetrahedra connected by common faces and corners.

The tetrahedra containing Cu, Fe, and Ge atoms vary in size. The Cu-centered tetrahedra have a mean Te...Te distance of 4.330(5) Å, which is slightly smaller than those containing Fe [4.442(6) Å] and Ge [4.531(5) Å], respectively. On the other hand, the tetragonal lattice distortion parameter ($\eta = c/2a$ = 1.00, as shown in Table II) indicates minimal lattice distortions in the crystal structure [36].

The interatomic bond distances Cu-Te [2.566(8) Å], Fe-Te [2.605(1) Å], and Ge-Te [2.552(8) Å] are smaller than the sum of the respective ionic radii (rCu^{+} = 0.71 Å, rFe^{2+} = 0.77 Å, rGe^{4+} = 0.53 Å, rTe^{2-} = 2.07 Å) for tetrahedrally bonded structures [37]. This reduction suggests an increased contribution of ionic interactions to bond formation. Nevertheless, these distances align well with those observed in other ternary and quaternary adamantane structures, including $CuInTe_2$ [38], Cu_2GeTe_3 [39], Cu_2SnTe_3 [40], Fe_2GeTe_4 [41], $Ag_2FeGaTe_4$ [15], $Cu_2ZnGeTe_4$ [42], $Cu_3In_5Te_9$ [43], and $Cu_3In_7Te_{12}$ [44]. These structures were identified in the Inorganic Crystal Structure Database (ICSD, release 2024.3) [45].

4. Conclusions

The diamond-like compound $Cu_2FeGeTe_4$ was synthesized using the melt and annealing technique through the direct reaction of its constituent elements. The thermal analysis of $Cu_2FeGeTe_4$ reveals a well-defined phase transition sequence, with the material remaining in the solid state up to 755 K, followed by a biphasic (solid + liquid) region up to 850 K, and complete melting above this temperature. The crystal structure was determined via powder X-ray diffraction. This material crystallizes in the non-centrosymmetric tetragonal space group $I-42m$, adopting a stannite structure. Its structure comprises a three-dimensional close-packed arrangement of slightly distorted $CuTe_4$, $FeTe_4$, and $GeTe_4$ tetrahedra, interconnected through shared faces and corners.

Acknowledgements

The authors thank Professor M. Quintero for providing the sample.

1. E. Parthé, Wurtzite and Sphalerite Structures, In J. H. Westbrook and R. L. Fleischer, eds., Crystal Structures of Intermetallic Compounds, Intermetallic Compounds, pp. 117-137 (J. Wiley, Chichester, 2000).

2. L. Pauling, The principles determining the structure of complex ionic crystals, *J. Am. Chem. Soc.* **51** (1929) 1010, https://doi.org/10.1021/ja01379a006

3. P. Valencia-Gálvez *et al.*, Cu2Zn(Sn1-xSix)Se4: Structural Characterization, Vibrational and Physical Properties of CZTSe- Derivatives, *Inorganics* **11** (2023), https://doi.org/10.3390/inorganics11010007

4. T. Zhu *et al.*, I2-II-IV-VI4 (I = Cu, Ag; II = Sr, Ba; IV = Ge, Sn; VI = S, Se): Chalcogenides for Thin-Film Photovoltaics, *Chem. Mater.* **29** (2017) 7868, https://doi.org/10.1021/acs.chemmater.7b02638

5. I. V. Bodnar *et al.*, Growing crystals and studying structure and electronic properties of $Cu_2ZnGe(S_xSe_{1-x})4$ compositions, *Heliyon* **9** (2023) e22533, https://doi.org/10.1016/j.heliyon.2023.e22533

6. H. Chen *et al.*, Transition-metal-based chalcogenides: A rich source of infrared nonlinear optical materials, *Coord. Chem. Rev.* **448** (2021) 214154, https://doi.org/10.1016/j.ccr.2021.214154

7. A. Hong, Y. Tang, and J. Liu, High-Throughput Screening of Quaternary Compounds and New Insights for Excellent Thermoelectric Performance, *J. Phys. Chem. C* **125** (2021) 24796, https://doi.org/10.1021/acs.jpcc.1c06843
8. S. Hall, J. Szymanski, and J. Stewart, Kesterite, Cu2(Zn,Fe)SnS4, and stannite, Cu2(Fe,Zn)SnS4, structurally similar but distinct minerals, *Can. Mineral.* **16** (1978) 131
9. E. Parthé, K. Yvon, and R. Deitch, High-Throughput Screening of Quaternary Compounds and New Insights for Excellent Thermoelectric Performance, *Acta Cryst. B* **25** (1969) 1164, https://doi.org/10.1107/S0567740869003670
10. C. Joubert-Bettan *et al.*, The crystal structures of Na2ZnSiO4, Na2ZnGeO4, and Na2MgGeO4, *J. Solid State Chem.* **1** (1969) 1, https://doi.org/10.1016/0022-4596(69)90001-2
11. C. D. Brunetta *et al.*, Cation ordering and physicochemical characterization of the quaternary diamond-like semiconductor Ag2CdGeS4, *J. Solid State Chem.* **187** (2012) 177, https://doi.org/10.1016/j.jssc.2011.12.032
12. O. Parasyuk *et al.*, The quasi-ternary system Ag2SCdSGeS2 and the crystal structure of Ag2CdGeS4, *J. Alloys Compd.* **397** (2005) 95, https://doi.org/10.1016/j.jallcom.2004.12.043
13. M. Quintero *et al.*, Crystallographic and Magnetic Properties of Cu2FeGeSe4 and Cu2FeGeTe4 Compounds, *phys. stat. sol. (b)* **209** (1998) 135, https://doi.org/10.1002/(SICI)1521-3951(199809)209:1⟨135::AID-PSSB135⟩3.0.CO;2-W
14. M. Quintero *et al.*, Crystallographic properties of I2-Fe-iv-vi4 magnetic semiconductor compounds, *Mater. Res. Bull.* **34** (1999) 2263, https://doi.org/10.1016/S0025-5408(00)00166-5
15. G. E. Delgado *et al.*, Synthesis and crystal structure of the quaternary compound AgFe2GaTe4, *J. Alloys Compd.* **613** (2014) 143, https://doi.org/10.1016/j.jallcom.2014.06.004
16. G. E. Delgado, L. Manfredy, and S. A. López-Rivera, Crystal structure of the ternary semiconductor Cu2In14/34/3Se8 determined by X-ray powder diffraction data, *Powder Diffr.* **33** (2018) 237, https://doi.org/10.1017/S0885715618000519
17. C. Chacón, P. Delgado-Niño, and G. Delgado, Synthesis and crystal structure determination of the new olivine-type compound Mn2SnSe4, *Rev. Mex. Fís.* **66** (2020) 30-34, https://doi.org/10.31349/RevMexFis.66.30
18. P. Delgado-Niño *et al.*, The Chalcogenide Compound Fe2SnSe4: Synthesis and Crystal Structure Analysis by Powder X-ray Diffraction, *Mater. Res.* **24** (2021) e20200142, https://doi.org/10.1590/1980-5373-MR-2020-0142
19. G. E. Delgado *et al.*, Synthesis and Crystal Structure of the Ordered Vacancy Compound Cu3In5Se9, *Orbital: Electron. J. Chem* **13** (2021) 236, https://doi.org/10.17807/orbital.v13i3.1560
20. G. E. Delgado and M. Quintero, Synthesis and structural characterization using the Rietveld method of the quaternary compound CuAlGeSe4, *Rev. Mex. Fís.* **68** (2022) 020501, https://doi.org/10.31349/RevMexFis.68.020501
21. T. Roisnel and J. Rodríguez-Carvajal, WinPLOTR: A Windows Tool for Powder Diffraction Pattern Analysis, *Mater. Sci. Forum* **378-381** (2001) 118-123, https://doi.org/10.4028/www.scientific.net/msf.378-381.118
22. S. Gates-Rector and T. Blanton, The Powder Diffraction File: a quality materials characterization database, *Powder Diffr.* **34** (2019) 352-360, https://doi.org/10.1017/S0885715619000812
23. A. Boultif and D. Louër, Powder pattern indexing with the dichotomy method, *J. Appl. Cryst.* **37** (2004) 724, https://doi.org/10.1107/S0021889804014876
24. A. D. Mighell, C. R. Hubbard, and J. K. Stalick, NBS'AIDS, Technical Note 1141, National Bureau of Standards, USA (1981).
25. P. M. de Wolff, A simplified criterion for the reliability of a powder pattern indexing, *J. Appl. Cryst.* **1** (1968) 108, https://doi.org/10.1107/S002188986800508X
26. G. S. Smith and R. L. Snyder, FN: A criterion for rating powder diffraction patterns and evaluating the reliability of powder-pattern indexing, *J. Appl. Cryst.* **12** (1979) 60, https://doi.org/10.1107/S002188987901178X
27. H. M. Rietveld, A profile refinement method for nuclear and magnetic structures, *J. Appl. Cryst.* **2** (1969) 65, https://doi.org/10.1107/S0021889869006558
28. J. Rodríguez-Carvajal, FullProf, version 8.20, Tech. rep., LLB, CEA-CNRS, France (2025).
29. A. Liu *et al.*, Selective synthesis and magnetic properties of FeSe2 and FeTe2 nanocrystallites obtained through a hydrothermal co-reduction route, *Solid State Comm.* **138** (2006) 538, https://doi.org/10.1016/j.ssc.2006.04.008
30. G. Caglioti, A. Paoletti, and F. Ricci, Choice of collimators for a crystal spectrometer for neutron diffraction, *Nucl. Instrum.* **3** (1958) 223, https://doi.org/10.1016/0369-643X(58)90029-X
31. P. Thompson, D. E. Cox, and J. B. Hastings, Rietveld refinement of Debye-Scherrer synchrotron X-ray data from Al2O3, *J. Appl. Cryst.* **20** (1987) 79, https://doi.org/10.1107/S0021889887087090
32. R. J. Hill and C. J. Howard, Quantitative phase analysis from neutron powder diffraction data using the Rietveld method, *J. Appl. Cryst.* **20** (1987) 467, https://doi.org/10.1107/S0021889887086199
33. I. D. Brown and D. Altermatt, Bond-valence parameters obtained from a systematic analysis of the Inorganic Crystal Structure Database, *Acta Cryst. B* **41** (1985) 244, https://doi.org/10.1107/S0108768185002063
34. N. E. Brese and M. O'Keeffe, Bond-valence parameters for solids, *Acta Cryst. B* **47** (1991) 192, https://doi.org/10.1107/S0108768190011041
35. I. D. Brown, Recent Developments in the Methods and Applications of the Bond Valence Model, *Chem. Rev.* **109** (2009) 6858, https://doi.org/10.1021/cr900053k

36. E. R. De Gil, Ternary semiconducting compounds with chalcopyrite-type structure: I. Fundamental equation and its physically acceptable solutions, *phys. stat. sol. (a)* **70** (1982) 519, https://doi.org/10.1002/pssa.2210700220

37. R. D. Shannon, Revised effective ionic radii and systematic studies of interatomic distances in halides and chalcogenides, *Acta Cryst. A* **32** (1976) 751, https://doi.org/10.1107/S0567739476001551

38. K. Knight, The crystal structures of CuInSe2 and CuInTe2, *Mater. Res. Bull.* **27** (1992) 161, https://doi.org/10.1016/0025-5408(92)90209-I

39. G. E. Delgado *et al.*, Structural refinement of the ternary chalcogenide compound Cu2GeTe3 by X-ray powder diffraction, *phys. stat. sol. (a)* **201** (2004) 2900, https://doi.org/10.1002/pssa.200406850

40. G. E. Delgado *et al.*, Crystal structure refinement of the ternary compound Cu2SnTe3 by X-ray powder diffraction, *Cryst. Res. Technol.* **43** (2008) 433, https://doi.org/10.1002/crat.200711049

41. G. Delgado *et al.*, Synthesis and crystallographic study of the ternary semiconductor compound Fe2GeTe4, *Chalcogenide Lett.* **7** (2010) 133

42. L. Nieves *et al.*, Structural characterization of the hightemperature modification of the Cu2ZnGeTe4 quaternary semiconductor compound, *phys. stat. sol. (b)* **253** (2016) 1195, https://doi.org/10.1002/pssb.201552782

43. G. E. Delgado *et al.*, Synthesis, structural study, and magnetic susceptibility of the chalcogenide olivine compound Mn2SiTe4, *JCCHEMS* **68** (2024) 5995.

44. G. E. Delgado *et al.*, Crystal structure and powder Xray diffraction data of the super-paramagnetic compound CuFeInTe3, *Rev. Mex. Fís.* **67** (2021) 305-311, https://doi.org/10.31349/RevMexFis.67.305

45. D. Zagorac *et al.*, Recent developments in the Inorganic Crystal Structure Database: theoretical crystal structure data and related features, *Journal of Applied Crystallography* **52** (2019) 918, https://doi.org/10.1107/S160057671900997X